Magnetic quenching of back scattering in coupled double quantum wires: giant mobility enhancement



1996 J. Phys.: Condens. Matter 8 L703

(http://iopscience.iop.org/0953-8984/8/46/001)

J. Phys.: Condens. Matter **8** (1996) L703–L710. Printed in the UK

**LETTER TO THE EDITOR**

# Magnetic quenching of back scattering in coupled double quantum wires: giant mobility enhancement

S K Lyo

Sandia National Laboratories, Albuquerque, NM 87185, USA

Received 27 August 1996, in final form 16 September 1996

**Abstract.** We show theoretically that the low-temperature mobility and conductance of thin double quantum wires formed from coupled double quantum wells can be enhanced by orders of magnitude by an applied magnetic field of a few tesla. This enhancement is caused by quenching of the intrawire back scattering which occurs when the Fermi level falls within the partial energy gap. The gap is created by the anticrossing of the energy dispersion curves of two quantum wires which are displaced relative to each other by the field.

Electron transport in quasi-one-dimensional (1D) quantum-well wires (QWWs) has received increasing attention recently [1–5]. The original interest in QWWs was conceived in search of high-mobility device structures for the possibility that the restricted phase space in 1D may reduce the momentum dissipation rate and increase the mobility [1]. In a 1D wire sufficiently thin that only the lowest 1D sublevel is occupied, momentum is dissipated through back scattering between two Fermi points at low temperatures ($T$). We propose a novel mechanism which enhances the low-$T$ mobility by orders of magnitude through quenching of the back scattering in the restricted 1D phase space. This enhancement is achieved in thin tunnel-coupled double quantum-well wires (DQWWs) by applying a magnetic field ($B$) in the growth plane (i.e., perpendicular to the plane containing both wires) in a direction ($\|x$) perpendicular to the two parallel QWWs. The dramatic and sharply $B$-dependent enhancement effect may eventually be useful for future device applications (e.g., magnetic switching), since it provides a technique for greatly increasing conductance.

The Hamiltonian is given in the effective mass approximation by

$$H = p_z^2/2m^* + \left(\hbar^2/2m^*\right)\left(k - z/l^2\right)^2 + V(z) \tag{1}$$

where the confinement potential $V(z)$ is the superposition of the square-well potentials $V_1(z)$ and $V_2(z)$ of QW1 and QW2. For simplicity, the QWs are assumed to be identical with well-widths $b$, depths $V$, and centre-to-centre distance $d$. We assume that the diameter of the QWWs is smaller than the classical magnetic length $l = (\hbar c/eB)^{1/2}$ in the range of $B$ of interest. The interest of this paper is in the limit where only the ground sublevels are populated. The total eigenfunction is given by $\Psi(x, y, z) = \varphi(x)L^{-1/2} \exp(-\mathrm{i}ky)\psi(z, k)$ where $L$ is the length of the wire ($\|y$) (assumed to be much shorter than the 1D weak localization length), $\varphi(x)$ is the confinement function in the direction of the field, and $\psi(z, k)$ is the eigenfunction of (1) in the growth direction ($\|z$).

Although some important properties of the eigenfunctions of (1) were discussed earlier by the present author [6], it is necessary to equip the readers with some of their basic properties to elucidate the theory. The eigenfunctions $\psi(z, k)$ are obtained by employing

0953-8984/96/460703+08$19.50  

tight-binding basis functions $\phi_1(z)$ and $\phi_2(z)$, which are the ground sublevel confinement functions of QW1 and QW2 alone. The energy eigenvalues $\varepsilon_k$ and the density of states (DOS) are displayed in figure 1 as solid curves at three magnetic fields $B = 0$, 4.8, and 6.0 T for a symmetric GaAs/$Al_{0.3}Ga_{0.7}$As DQWW structure with $m^* = 0.067\ m_0$ in the QWs ($m_0$ is the free-electron mass), $m^* = 0.073\ m_0$ in the barriers, $b = 8$ nm, $d = 14$ nm, and the well depths $V_0 = 280$ meV. The black dots at the tips of the double-sided arrows denote the Fermi points and the dotted horizontal lines in the DOS figures signify the position of the chemical potential ($\mu$) for the 1D electron density $N_{1D} = 6.5 \times 10^5$ cm$^{-1}$. While only symmetric DQWWs are discussed and studied numerically in this paper, a similar argument can be extended to an asymmetric structure with minor changes. Our formal result for the conductance is, however, applicable to a general situation.

A useful intuitive understanding of the eigenvalues and eigenfunctions is gained by initially turning off the tunnelling between the QWs: the unperturbed in-plane eigenvalues

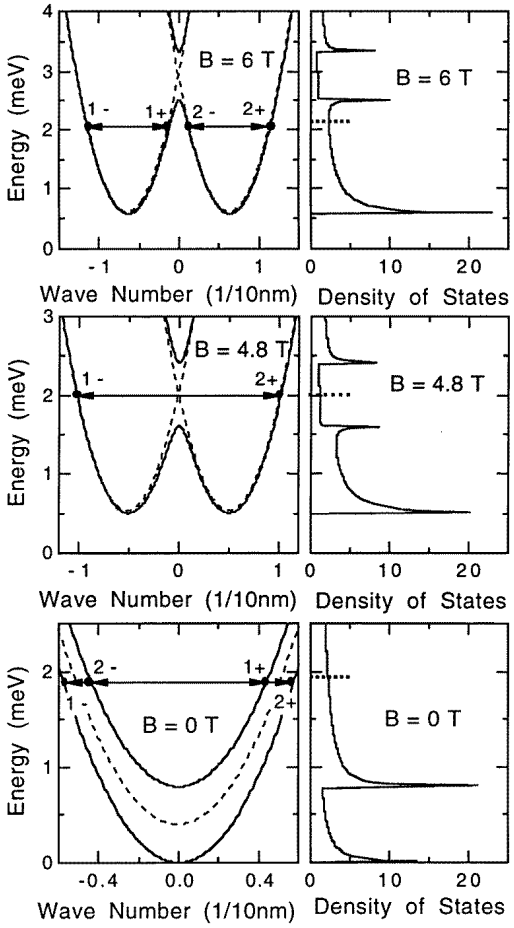


**Figure 1.** The energy eigenvalues (solid curves) and the DOS. The dashed curves are the unperturbed parabolas. The arrows indicate back scattering between the Fermi points (black dots). Dotted lines in the DOS figures indicate the chemical potentials. The +, − signs signify the signs of the slopes at the Fermi points.

in QW1 and QW2 are indicated by the dashed parabolas in figure 1. The bottoms of these parabolas rise in energy with increasing $B$ due to the diamagnetic shift. At $B = 0$ T, the two parabolas coincide. This degeneracy is removed by $B$ at all $k$ except at the crossing point at $k = 0$, as the two parabolas are shifted relative to each other by the amount $\Delta k = dl^{-2}$ as can be seen readily from (1). When the tunnelling is turned on, the degeneracy at $k = 0$ is removed and a gap is opened as shown by the solid curves.

At $B = 0$, the two solid parabolas represent symmetric–antisymmetric splitting with energy $\Delta_{SAS} = 0.8$ meV. The DOS is proportional to $\varepsilon^{-1/2} + (\varepsilon - \Delta_{SAS})^{-1/2}$. The wave functions are given by $\psi(z, k) = [\phi_1(z) \pm \phi_2(z)]/[2(1 \pm S)]^{1/2}$ for all $k$. Here $S = \langle\phi_1(z)|\phi_2(z)\rangle$ is the overlap integral. In the symmetric case discussed here, the wave functions have equal probability distribution on each QW. For the purpose of a later analysis, numbers 1 and 2 are assigned in figure 1 to the Fermi points, according to the original positions of these points on the unperturbed parabolas at $B > 0$. The signs +, − following the numbers indicate the signs of the slopes (i.e., the group velocities).

The crossing point of the two dashed parabolas rises in energy with increasing $B$. The gap rises at the same time and passes through $\mu$ as shown in figure 1. The gap energy is insensitive to $B$. It is important to point out here that, at high $B$ with $\mu$ below the gap (e.g., at $B = 6$ T in figure 1), $\psi(z, k)$ approaches asymptotically the unperturbed confinement functions $\phi_1(z)$ and $\phi_2(z)$ at the Fermi points $1\pm$ and $2\pm$, respectively. Similarly, when $\mu$ is within the gap (e.g., at $B = 4.8$ T), $\psi(z, k)$ is $\phi_1(z)$-like at the Fermi point $1-$ and $\phi_2(z)$-like at $2+$ as seen by the fact that the solid dispersion curve coincides with the dashed parabola of QW1 at $1-$ and with that of QW2 at $2+$. The origin of this spatial separation of the forward-moving and backward-moving electrons in the gap is the Lorentz force.

We now introduce a qualitative discussion of the quenching mechanism of the intrawire scattering and the accompanying giant mobility enhancement, before carrying out a formal analysis. When $\mu$ is outside the gap (e.g., at $B = 0$ and 6 T in figure 1), the dominant back scattering occurs within the wire. Because of the wide barrier, only a minor contribution occurs from interwire scattering. In contrast, when $\mu$ is inside the gap (e.g., at $B = 4.8$ T), back scattering occurs predominantly through the barrier, because the wave functions at the Fermi points $1-$ and $2+$ are separated into QW1 and QW2, respectively, as discussed already. The spatial separation of the wave functions for $1-$ and $2+$ produces a greatly reduced probability of scattering. As a result, the scattering rate drops abruptly as the upper gap edge sweeps across the Fermi level, yielding a large mobility enhancement. This kind of drastic quenching of intrawire scattering is unique to the 1D structure, due to its limited phase space with only two Fermi points. By contrast, in two-dimensional (2D) double QWs, electrons can move freely within the extra degree of freedom in the $x$-direction. The Fermi surface then consists of a 2D orbit inside the gap. Scattering can occur between any two points of this 2D orbit and is not necessarily 180° back scattering, yielding no such dramatic effect inside the gap [6–8]. When more than one 1D sublevel is occupied, the enhancement arises from quenching of the back scattering between one pair of in-gap Fermi points of a sublevel and will be greatly reduced, because intrawire back scattering is still available for other Fermi points of other occupied sublevels which are outside the gap.

The conductance is given, ignoring spin splitting, by

$$G(B) = \frac{2e^2}{L^2} \sum_k v_k \left[-f'\left(\varepsilon_k\right)\right] g_k \tag{2}$$

where $v_k = \mathrm{d}\varepsilon_k/\hbar\,\mathrm{d}k$ is the group velocity, $e$ is the electronic charge, and $f'(x)$ is the first derivative of the Fermi function. In (2), the mean free path $g_k = v_k\tau_k$ ($\tau_k$ is the transport

relaxation time) is obtained from the Boltzmann equation:

$$v_k + \frac{2\pi N_{imp} L}{\hbar} \sum_{k'} V(k, k')^2 (g_{k'} - g_k)\delta(\varepsilon_k - \varepsilon_{k'}) = 0 \tag{3}$$

where $N_{imp}$ is the 1D impurity density and $V(k, k')^2$ is the square of the absolute value of the scattering matrix element averaged over the impurity distribution. The $k$- and $k'$-summations in (2) and (3) include both branches of the eigenvalues. The effect of spin splitting will be discussed later.

At low $T$, the $k$- and $k'$-summations in (2) and (3) become discrete sums over four Fermi points when $\mu$ is outside the gap and two Fermi points when it is inside the gap. The conductance in (2) is then simplified to

$$G(B) = e^2 g/(\pi h L) \tag{4}$$

where $g$ is the sum of mean free paths $g_{k_i}$ over all the Fermi points $k_i$. The Boltzmann equation in (3) can also be rewritten as coupled equations of mean free paths $g_k$ on the discrete Fermi points. The quantity $g$ is given in units of $\hbar^2/(L^2 N_{imp})$ by

$$\begin{aligned} g &= u^{-1}_{1-,2+} \qquad \text{(two Fermi points)} \\ &= F/D \qquad \text{(four Fermi points)} \end{aligned} \tag{5}$$

where $u_{i,j} = u_{j,i} = V(k_i, k_j)^2/|v(k_i)v(k_j)|$, $v(k) = v_k$, and $k_i$, $k_j$ are wave numbers at the Fermi points. The quantity $F$ is given by

$$\begin{aligned} F = {} & (u_{1-,2+} + u_{1+,2+})(u_{1-,2+} + u_{1+,2-}) + (u_{1-,1+} + u_{2-,2+}) \\ & \times (u_{1-,2-} + u_{1-,2+} + u_{1+,2-} + u_{1+,2+}) + 4u_{1-,2-}u_{1+,2+} \end{aligned} \tag{6}$$

and $D$ is the determinant of a $3 \times 3$ matrix:

$$D = \begin{vmatrix} u_{1-,1+} + u_{1-,2-} + u_{1-,2+} & u_{1-,2+} & -u_{1-,2-} \\ u_{1-,2+} & u_{1-,2+} + u_{2-,2+} + u_{1+,2+} & u_{2-,2+} \\ -u_{1-,2-} & u_{2-,2+} & u_{1-,2-} + u_{1+,2-} + u_{2-,2+} \end{vmatrix}. \tag{7}$$

The subscripts $1\pm$ and $2\pm$ in (5)–(7) indicate $k$ at the Fermi points designated by these symbols in figure 1.

In order to demonstrate the conductance enhancement, we calculate $G(B)$ for the sample studied in figure 1 using (4)–(7) for short-range delta-function-potential scattering centres (designated by black dots) uniformly distributed along the wires on two of the interfaces of the QWs as illustrated in the inset of figure 2. This example is relevant to high-mobility QWWs where surface roughness scattering is dominant [4]. Discussions of the effect of other elastic and inelastic scattering will be given later. The total number of scattering centres is the same in the four cases studied in figure 2. The fractional numbers in the inset therein indicate the fractional distribution of the scattering centres. The conductance is inversely proportional to $|\langle\varphi(x)|c(x)|\varphi(x)\rangle|^2$ where $c(x)$ denotes the impurity distribution in the $\boldsymbol{B}$-direction on the interfaces. Information on the scattering strength and the confinement function $\varphi(x)$ is not necessary because we are interested only in the relative conductance. The zero-$B$ conductances for the four cases are approximately equal with less than 1% differences owing to the fact that the zero-$B$ wave functions are shared equally between the two QWs.

The conductance enhancement ($\equiv G(B)/G(0)$) between 4.4 and 5.2 T is shown in figure 2 for the four cases and is striking. This gigantic enhancement is due to the quenching of intrawire back scattering when $\mu$ is within the gap as discussed above. The enhancement

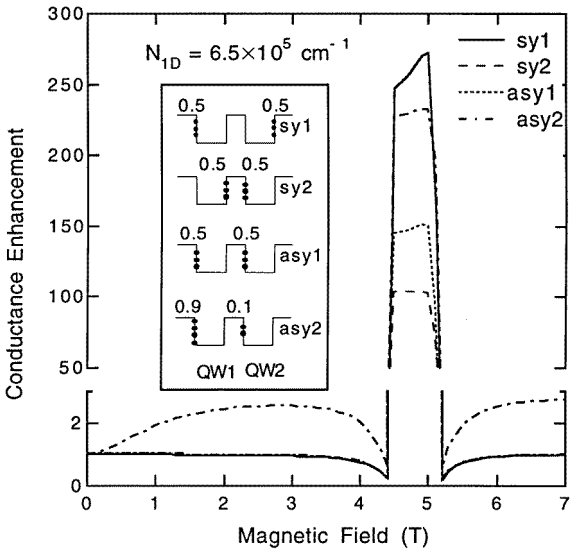


**Figure 2.** Conductance enhancement $G(B)/G(0)$ against $B$ for 8–6–8 nm DQWWs. The inset shows four configurations of scattering centres. Other parameters are given in the text. Note that the vertical axis is split with two different scales.

$G(B)/G(0)$ is nearly equal outside the gap in cases sy1, sy2, and asy1. In these cases, $G(B)$ decreases monotonically with increasing $B$ until it vanishes at the upper gap edge, where it jumps abruptly, reaches a maximum, and then drops again abruptly to zero at the lower gap edge. The conductance then increases monotonically, eventually saturating at the value corresponding to the conductance of the two uncoupled QWWs. However, our 1D model breaks down at very high $B$ where $l < b$ (e.g., $B > 10.3$ T in figure 3). In this case, the electrons are still confined in the $x$-direction and execute 2D cyclotron motion in the $y$–$z$-plane inside each QW, undergoing scattering and tunnelling at the interfaces of the wells. The vanishing of $G(B)$ at the gap edges is due to divergent scattering rates caused by the diverging DOS (in the absence of damping).

Spin splitting causes displacement of both the energy-dispersion curves and the gaps (figure 1) by the Zeeman splitting for the two spin states. In this case, $\mu$ first falls, with increasing $B$, into the gap of the higher-energy spin states, then into that of the lower-energy spin states, and finally exits the gaps. Neglecting spin-flip scattering, the current is carried by two independent noninteracting parallel channels. When the spin splitting is neglected, the quantity $G(B)/G(0)$ in figure 2 is the superposition of the two identical contributions (i.e., half of $G(B)/G(0)$ shown in figure 2) from each spin channel. In the presence of spin splitting, however, the turn-on and turn-off magnetic fields for the giant enhancement peaks are displaced for the two spin channels. As a result, the full enhancement peaks and return to the baseline value shown in figure 2 are achieved in two approximately equal steps if $\mu$ falls into the energy gap of the second spin states before exiting that of the first spin states (i.e., for large gap energy). If $\mu$ falls into the energy gap of the second spin states after exiting that of the first spin states (i.e., for small gap energy), the two enhancement peaks from the two spin channels (which are about half of those shown in figure 2) do not overlap.

The conductance behaves very differently in case asy2: it rises initially to a maximum

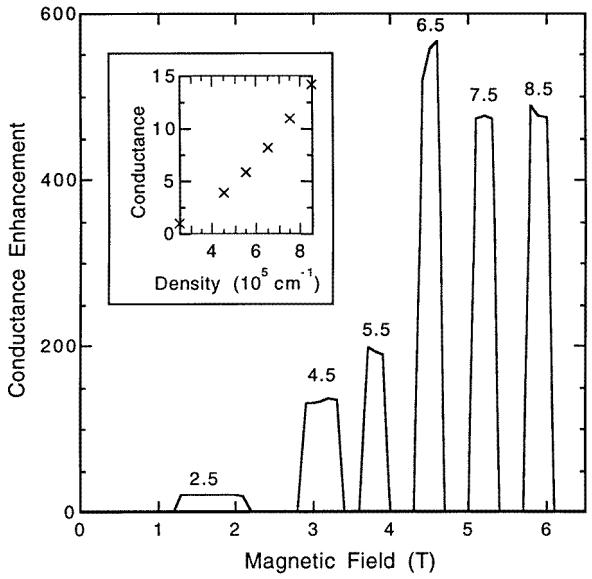


**Figure 3.** Conductance enhancement $G(B)/G(0)$ against $B$ for 8–7–8 nm DQWWs with a wider barrier than in figure 2 for the asy1 distribution of the scattering centres in the inset of figure 2. The numbers above each peak denote $N_{1D}$ in units of $10^5$ cm$^{-1}$. The inset shows $G(0)$ (in arbitrary units) against $N_{1D}$.

value before it starts a $B$-dependent behaviour similar to that in the above three cases. This initial rise is due to the resistance resonance between QW1 and QW2 with unequal zero-$B$ mobilities [9]. At $B = 0$, the rough interface of QW1 (with 90% of the total roughness) reduces the mobility of QW2 because $\psi(z, k)$ is shared equally between the two channels. As $B$ is increased, the wave functions begin to separate into QW1 and QW2 so that the said roughness scatters the electrons in QW2 much less. Therefore, the mobility of QW2 with only 10% of the total roughness becomes much larger than that of QW1, resulting in a larger flow of the current through QW2 and yielding larger $G(B)$. An extreme limit of this behaviour is reached at very high $B$, where QW1 and QW2 become uncoupled at the Fermi level, yielding a saturation $G(B)$ significantly larger than $G(0)$ as seen from the dash–dotted curve in figure 2.

The different peak heights in the four cases in figure 2 can also be understood from the spatial separation of the wave functions inside the gap into QW1 and QW2. The scattering rate proportional to $|\langle\psi(z, k_{1-})|V|\psi(z, k_{2+})\rangle|^2 \sim |\langle\phi_1(z)|V|\phi_2(z)\rangle|^2$ is the smallest in case sy1, because the scattering centres on the left interface of QW1 (right interface of QW2) are farthest from the wave function $\phi_2(z)$ ($\phi_1(z)$), yielding the largest enhancement (solid curve). Applying a similar logic, case sy2 yields the smallest enhancement (dashed curve). The asymmetric cases asy1 and asy2 belong to intermediate situations and may be more relevant to real samples, where surface roughness is known to be more severe in growing from an AlGaAs region into a GaAs region (from left to right in the inset of figure 2). The large enhancement shown by the dash–dotted curve corresponds to case asy2 where 90% of the interface roughness is on the left interface of QW1. In this case, the said roughness, being very far from QW2, is ineffective for back scattering through the barrier.

The enhancement can further be increased by increasing the barrier width as

demonstrated in figure 3. Here, the sample is identical to that used for figure 2 with an asy1-type distribution of the scattering centres but with a wider barrier width, 7 nm, and with a smaller gap energy, 0.41 meV. The numbers assigned to each peak denote $N_{1D}$ in units of $10^5$ cm$^{-1}$. The enhancement tends to increase with increasing $N_{1D}$, because the upper gap edge sweeps through $\mu$ at a higher $B$ where the separation of the wave functions inside the gap becomes more severe. However, this argument is only qualitative because other factors such as the velocity and the DOS affect the quantitative results. The enhancement can disappear if the gap is smeared by damping. Inside the gap, damping arises mainly from the forward scattering and is smaller than that outside the gap. The inset in figure 3 shows $G(0)$ as a function of the carrier density. In the above discussions, we have implicitly assumed that the wire is longer than the mean free path ($\sim g$), namely that the maximum of $G(B)$ is smaller than the maximum conductance $G_{\max}$. The latter is given by $G_{\max} = 2e^2/h$ inside the gap [10] and corresponds to $g = L$ in (4).

We have ignored a small forward-scattering contribution to the momentum relaxation. The latter arises from the $k'$-integration near the Fermi points $k' \sim k = k_{1-}, k_{2+}$ in the second term of (3) and vanishes for delta-function energy conservation. The effect of level broadening is estimated by replacing the delta function by a Lorentzian function with a width $w$. The magnitude of this term is then estimated by inserting the zeroth-order $g_{k'}$ and approximating $\varepsilon_{k'} = \hbar^2(k' \pm \Delta k/2)^2/2m^*$ near $k' = k_{2+}$ and $k_{1-}$, respectively: the ratio of this contribution to the first term in (3) is roughly $\delta = 5 \times 10^{-2}\eta w/\varepsilon_F$, where $\varepsilon_F$ is the Fermi energy and $\eta = u_{2+,2+}/u_{1-,2+}$ is of the order of the in-gap enhancement. Therefore, the results in (5)–(7) and figures 2 and 3 are valid for narrow level widths $w$ (i.e., $\delta \ll 1$).

At high $T$ ($k_BT \gg \Delta_{SAS}$), the in-gap enhancement is reduced approximately by a factor $\Delta_{SAS}/k_BT$ due to thermal excitation of the electrons to the low-conductance regions above the gap. A significant reduction of the enhancement can also arise from the lattice scattering of the electrons [3, 5] at high $T$. On the other hand, when $\mu$ is below the gap (e.g., at 6 T in figure 1), the carriers are activated into the gap, yielding enhanced conductance.

The low-$T$ enhancement effect discussed in this letter is not restricted to short-range impurity scattering but is applicable to a general class of scattering such as long-range Coulomb or electron–phonon scattering, because the enhancement mechanism relies mainly on the small overlap of the confinement functions of the two QWs involved in the back scattering inside the gap. More detailed results will be presented elsewhere.

In summary, we have proposed that the low-$T$ mobility of coupled thin DQWWs can be enhanced by orders of magnitude by an applied $B$ of a few tesla. This enhancement is caused by the quenching of intrawire back scattering which occurs when $\mu$ falls within the partial energy gap created by $B$-induced anticrossing of the energy dispersion curves of two quantum wells.

The author thanks J A Simmons for a careful reading of the manuscript and valuable discussions. This work was supported by US DOE contract No DE-AC04-94AL85000.

## References

[1] Sasaki H 1980 *Japan. J. Appl. Phys.* **19** L735
[2] Tanatar B and Gold A 1995 *Phys. Rev.* B **52** 1996
[3] Mickevicius R and Mitin V 1993 *Phys. Rev.* B **48** 17 194
[4] Motohisa J and Sakaki H 1992 *Appl. Phys. Lett.* **60** 1315
[5] Nag B R and Gangopadyhyay S 1995 *Semicond. Sci. Technol.* **10** 813
[6] Lyo S K 1994 *Phys. Rev.* B **50** 4965
[7] Simmons J A, Lyo S K, Harff N E and Klein J F 1994 *Phys. Rev. Lett.* **73** 2256

[8] Kurobe A, Castleton I M, Linfield E H, Grimshaw M P, Brown K M, Ritchie D A, Pepper M and Jones G A C 1994 *Phys. Rev.* B **50** 4889
[9] Palevski A, Beltram F, Capasso F, Pfeiffer L N and West K W 1990 *Phys. Rev. Lett.* **65** 1926
[10] Beenakker C W and van Houten H 1991 *Solid State Physics: Semiconductor Heterostructures and Nanostructures* vol 44, ed H Ehrenreich and D Turnbull (New York: Academic) p 111